Quantum critical point and unusual phase diagram in the itinerant-electron metamagnet UCoAl

N. Kimura,* N. Kabeya, and H. Aoki
Center for Low Temperature Science, Tohoku University, Sendai 980-8578, Japan
and Department of Physics, Graduate School of Science, Tohoku University, Sendai 980-8578, Japan

K. Ohyama, M. Maeda, H. Fujii, M. Kogure, and T. Asai
Department of Physics, Graduate School of Science, Tohoku University, Sendai 980-8578, Japan

T. Komatsubara, T. Yamamura, and I. Satoh
Institute for Materials Research, Tohoku University, Sendai 980-8577, Japan
(Received 27 October 2014; published 2 July 2015)

We present the temperature–pressure–magnetic-field phase diagram of the itinerant-electron metamagnet UCoAl determined from the ac susceptibility measurement. The quantum critical point (QCP) was found to be located at 2.9 ± 0.2 GPa ($\equiv P_{\mathrm{QCP}}$) and 130 ± 5 kOe. In addition to the determination of the phase diagram, we report magnetic and transport properties in the paramagnetic state and around the phase boundary. The critical divergence of the magnetic susceptibility is suppressed toward the QCP. From the longitudinal magnetoresistance and the resistivity under magnetic fields, enhancement of the resistivity is observed in the so-called supercritical region. In the paramagnetic region, the magnetoresistance and temperature dependence of the resistivity exhibit complex behaviors, especially in the vicinity of 1.5 GPa and P_{QCP}.

DOI: 10.1103/PhysRevB.92.035106 PACS number(s): 75.30.Kz, 74.40.Kb, 71.10.Hf, 74.62.Fj

I. INTRODUCTION

Quantum criticality is one of the most intriguing phenomena in condensed matter physics. For example, some heavy-fermion compounds exhibit an unconventional superconductivity in the vicinity of the quantum critical point (QCP), where the antiferromagnetic ordering temperature can be brought to zero by controlling an external parameter such as pressure [1]. Additionally, an unconventional Fermi-liquid (FL) behavior and superconductivity are often observed in this quantum critical region. Superconductivity on the border of a magnetic order is also observed in some itinerant-electron ferromagnets [2,3]. In such a system, the ferromagnetic transition temperature, i.e., the Curie temperature, decreases with increasing pressure (P) and the magnetic transition changes from second order (continuous) to first order (discontinuous) at a tricritical point. At this stage, the transition temperature reaches zero at the quantum phase transition point (QPTP). Above the pressure of the QPTP, the magnetic ground state is paramagnetic, and a metamagnetic transition of the first order appears with application of a magnetic field (H). The critical temperature (T_{cr}) of the metamagnetic transition decreases with increasing P and reaches zero at the QCP. An exotic magnetic state is expected at the QCP, and the appearance of a magnetic nematic phase has actually been confirmed in $Sr_3Ru_2O_7$ [4], for which the metamagnetic transition is thought to be situated near the QCP [5]. Therefore, investigation of how such an exotic state emerges from the QPTP toward the QCP promises to yield rich and interesting insights into the magnetism of itinerant-electron systems.

UCoAl is well known as an itinerant-electron paramagnet, with the metamagnetic transition occurring at 0.5 T [6,7]. The crystal structure is a ZrNiAl-type $P\bar{6}2m$ (no. 189, D_{3h}^3) hexagonal structure [8], known as the so-called quasi-kagome lattice without inversion symmetry. The band metamagnetism of UCoAl is governed by $5f$ electrons [8], which indicates that the $5f$ electrons become itinerant. The nonlocal marginal-Fermi-liquid (NLMFL) variation [9] as $T^{5/3}$ in the electrical resistivity $\rho(T)$ is observed below the metamagnetic transition field H_m, while the conventional FL variation as T^2 is restored above H_m [10]. Application of pressure increases H_m by 0.027 T/GPa [11]. The QPTP where $H_m \to 0$ is expected to be situated at a slightly negative pressure (≈ -0.3 GPa) [12]. Therefore, UCoAl is one of the most suitable candidates for investigating magnetic evolution from the QPTP toward the QCP.

In a previous study, Aoki *et al.* determined the T-P-H phase diagram and QCP to be 1.5 GPa and 60 kOe from magnetostriction and transverse magnetoresistance (MR) measurements [13]. In this paper, we present a similar but different phase diagram determined from the ac magnetic susceptibility which can define the critical point (CP) more definitely and directly. Comparing these phase diagrams, we reveal that UCoAl does not exhibit the simple magnetic phase diagram initially expected. We also report the unusual behavior of the electrical resistivity in the paramagnetic phase.

II. EXPERIMENT

Single crystals of UCoAl were grown by the Czochralski pulling method in a tetra-arc furnace. The residual resistivity and its ratio were 7.5 $\mu\Omega$ cm and 15, respectively. These values are almost the same as those in previous reports [7,14], guaranteeing that the present samples were of sufficient quality.

Pressure was applied up to 2.94 GPa by a BeCu/NiCrAl clamped piston-cylinder cell with a 1:1 mixture of 1- and 2-propanol as the pressure-transmitting medium. The same setup was successfully used for de Haas–van Alphen experiments

*kimura@mail.clts.tohoku.ac.jp

under pressure, indicating that hydrostatic pressures of high quality can be achieved [15]. The pressures at low temperatures were determined by the resistivity of Manganin wire which was calibrated against the ac susceptibility drop of the superconducting transition of Sn. We used a ^{4}He cryostat equipped with a 10 T superconducting magnet for measurements at temperatures above 1.5 K and a dilution refrigerator with a 17 T superconducting magnet for measurements at temperatures below 1.8 K. A RuO_2 thermometer that is calibrated under magnetic fields was put on the level of the sample. We selected an appropriate sweep rate of the magnetic field ($\leqslant$1 kOe/min) to avoid self-heating of the pressure cell. The ac susceptibility was measured with the dc and ac magnetic fields parallel to the c axis. The frequency and amplitude of the ac field were 7 Hz and 10 Oe, respectively. The resistivity measurements were performed by a conventional four-probe dc method with current $j = 2\,\mathrm{A/cm^2}$. An ac method with $j = 0.06\,\mathrm{A/cm^2}$ (rms) was employed for the measurements in the dilution refrigerator below 1.8 K. The magnetic field and current were applied along the c axis. In order to check the dc magnetization, we utilized a magnetic property measurement system (MPMS-XL) by Quantum Design Co. Ltd.

The samples for the ac susceptibility and resistivity (longitudinal MR) measurements were rectangular in shape and their dimensions were $0.75 \times 0.75 \times 4.35\,\mathrm{mm^3}$ and $0.38 \times 1.29 \times 3.11\,\mathrm{mm^3}$, respectively. The long axis of both samples was parallel to the c axis. Their demagnetization factors were thus small. Considering the small size of the magnetic moment in comparison to the applied magnetic fields, we can neglect the demagnetization effect in the present study. (The demagnetization field is estimated to be on the order of 100 Oe.)

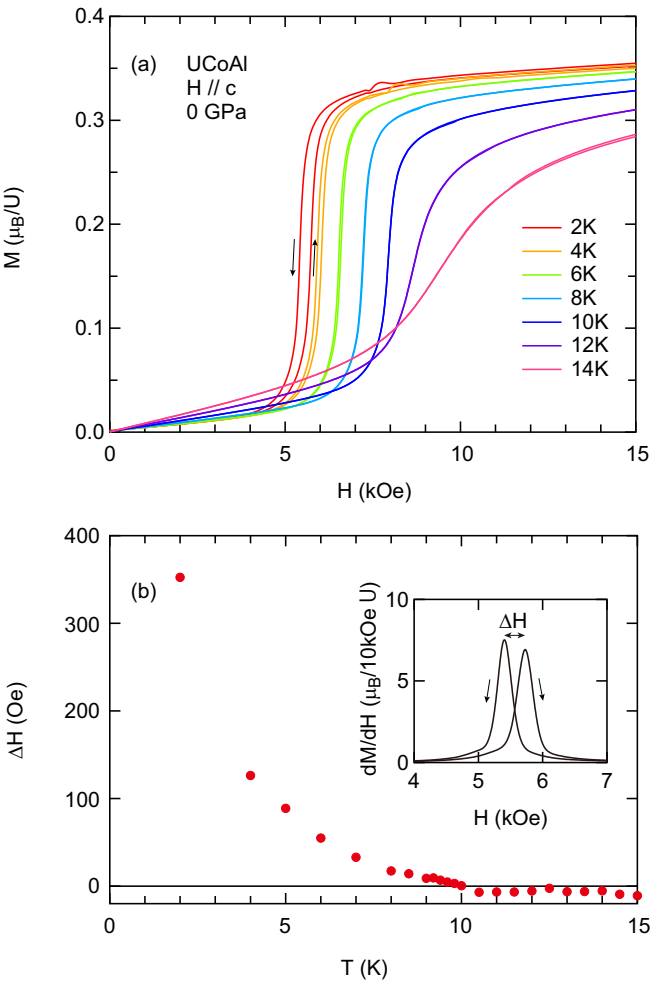

FIG. 1. (Color online) (a) Temperature variation of the magnetization curves of UCoAl for $H \parallel c$ at 0 GPa. (b) Temperature dependence of the hysteresis width ΔH, which is defined as the difference between the peak fields of dM/dH in the up and down sweeps indicated in the inset. Negative values of ΔH above 10 K are probably due to an inevitable hysteresis of the superconducting magnet in an MPMS.

III. RESULTS

A. Determination of the critical point

Figure 1(a) shows the temperature variation of the magnetization curves. Both increasing and decreasing processes are plotted. The magnetization at 2 K rapidly increases at approximately 5.5 kOe, indicating the metamagnetic transition. A hysteresis behavior manifests itself, indicating that the metamagnetic transition is of first order. With an increase in temperature, the transition becomes less abrupt, and the hysteresis becomes less pronounced. These features indicate that the first-order transition changes to a crossover through the critical point with increasing temperature. The CP is defined as the termination point of the transition line between the paramagnetic and polarized phases. The hysteresis of the first-order transition should vanish at the CP. To determine the CP from the magnetization measurement, we estimate the hysteresis width $\Delta H \equiv H_{\mathrm{up}} - H_{\mathrm{down}}$, where $H_{\mathrm{up\,(down)}}$ is the field at which $dM_{\mathrm{up\,(down)}}/dH$ peaks [see the inset of Fig. 1(b)]. As shown in Fig. 1(b), ΔH drops to zero at 10 K. From this we determine that the CP is $(T_{\mathrm{cr}}, H_{\mathrm{cr}}) = (10.5 \pm 0.5\,\mathrm{K}, 8.1 \pm 0.1\,\mathrm{kOe})$, with T_{cr} and H_{cr} representing the critical temperature and field, respectively. These values are consistent with the previous report [16].

The above procedure is a simple way to determine the CP. However, measurement of the magnetization under pressure is technically difficult, especially at very low temperatures. The above method based on the magnetization is not applicable for determining the QCP. Therefore, instead of measuring the magnetization, we went on to perform an ac susceptibility measurement, which permitted us to reach temperatures as low as 0.03 K. Moreover, the ac susceptibility can determine the CP more accurately than the magnetization and/or other thermodynamic measurements. In the magnetization measurement, ΔH narrows asymptotically with increasing temperature, as shown in Fig. 1(b), which gives an ambiguity to the determination of the CP. On the other hand, the ac susceptibility is very sensitive to the existence of the hysteresis, as shown later [Fig. 2(b)]. One may consider that a MR, which is also measurable down to 0.03 K, is a suitable method for determining the QCP. However, the MR may not capture properly the magnetic criticality since it is not a thermodynamic variable. Influences other than the magnetic criticality can possibly affect it.

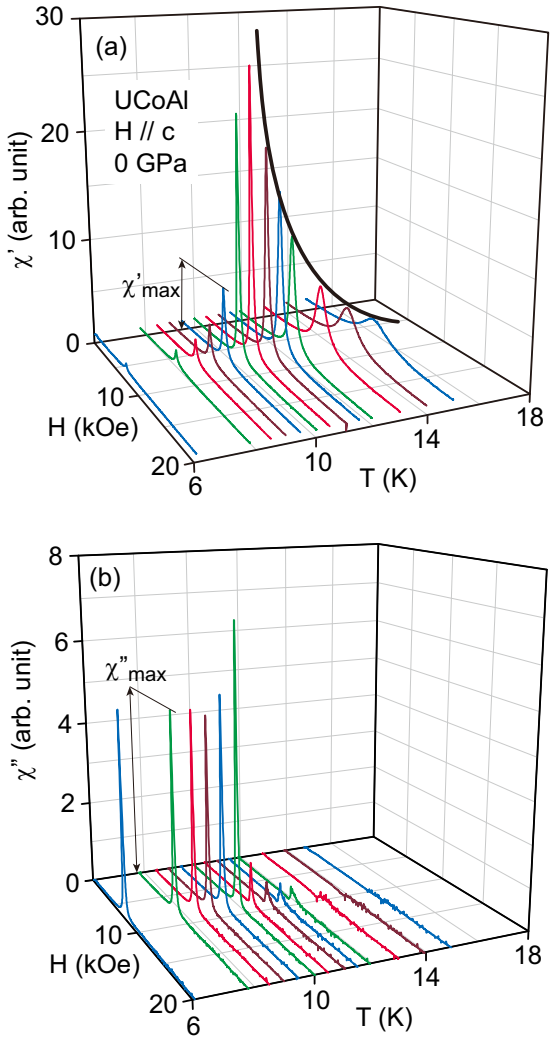

FIG. 2. (Color online) Real (a) and imaginary (b) parts of the ac susceptibility, χ' and χ'', respectively, as functions of the field for various temperatures at 0 GPa.

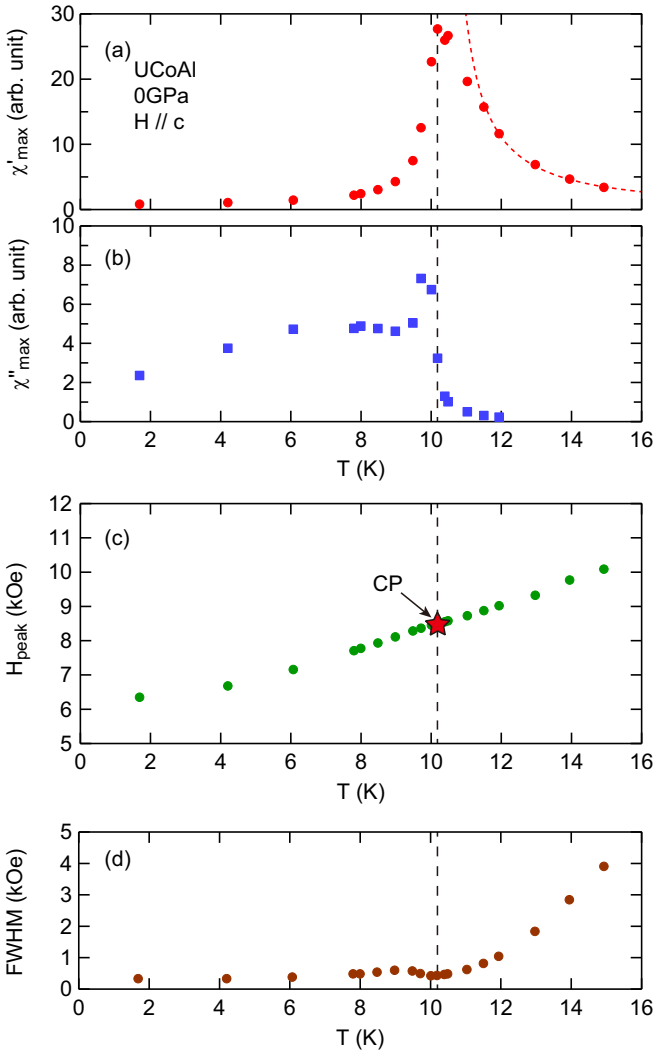

FIG. 3. (Color online) Temperature dependence of characteristic parameters at 0 GPa; (a) $\chi'_{\rm max}$ and (b) $\chi''_{\rm max}$ are defined as the maximum values of $\chi'(H)$ and $\chi''(H)$ at each temperature. (c) $H_{\rm peak}$ is the field where $\chi'(H) = \chi'_{\rm max}$. (d) The full width at half maximum (FWHM) of the peak in $\chi'(H)$, which reflects the transition width. The broken lines in every graph indicate $T_{\rm cr}$ and the red star in (c) indicates $H_{\rm cr}$.

Figure 2(a) shows the field dependence of the real part of the ac susceptibility, χ', for selected temperatures. The metamagnetic transition (and crossover) is observed as a peak in $\chi'(H)$. The peak of $\chi'(H)$ grows continuously and diverges from high temperatures to $T_{\rm cr}$, as indicated by the bold curve in Fig. 2(a). A rapid decline in the peak of $\chi'(H)$ below $T_{\rm cr}$ is due to the hysteresis and/or irreversibility of the magnetization process in the vicinity of the metamagnetic transition. The imaginary part of the ac susceptibility $\chi''(H)$ measures an energy loss that is proportional to the area enclosed by the hysteresis loop during one cycle of the ac field. As shown in Fig. 2(b), $\chi''(H)$ exhibits a peak below $T_{\rm cr}$, indicating the hysteresis in the magnetization process. The peak of $\chi''(H)$ is suddenly suppressed above $T_{\rm cr}$ and disappears above 12 K.

The temperature dependences of the peak heights of $\chi'(H)$ and $\chi''(H)$, $\chi'_{\rm max}$ and $\chi''_{\rm max}$, are plotted in Figs. 3(a) and 3(b), respectively. $\chi'_{\rm max}(T)$ shows a peak and $\chi''_{\rm max}(T)$ drops at the same temperature of 10.2 K, indicating that $T_{\rm cr}$ is 10.2 K. The broken curve in Fig. 3(a) represents the critical divergence of the susceptibility with the critical exponent $\gamma = 1.2$, determined by NMR measurement [17]. $\chi'_{\rm max}(T)$ deviates from the expected curve in the temperature range from 12 K to $T_{\rm cr}$. A finite value of $\chi''_{\rm max}$ also remains in the same temperature range. These deviations from the ideal behaviors are probably due to inhomogeneity of the sample and/or a nonuniform internal field in the nonellipsoidal sample shape. As shown in Fig. 3(a), at $T_{\rm cr}$, $\chi'(H)$ peaks at 8.5 kOe. Consequently, the CP is determined to be $(T_{\rm cr}, H_{\rm cr}) = (10.2 \pm 0.5\ {\rm K}, 8.5 \pm 0.1\ {\rm kOe})$. The $T_{\rm cr}$ obtained is consistent with the result of the magnetization measurement.

Figure 3(c) shows the temperature dependence of the peak position $H_{\rm peak}$ where $\chi'(H) = \chi'_{\rm max}$. Strictly speaking, $H_{\rm peak}$ below $T_{\rm cr}$ does not necessarily correspond to the thermodynamic metamagnetic-transition field H_m, but we regard $H_{\rm peak}$ as H_m in the present study. $H_{\rm peak}(T)$ below $T_{\rm cr}$ indicates the metamagnetic transition line, whereas $H_{\rm peak}(T)$

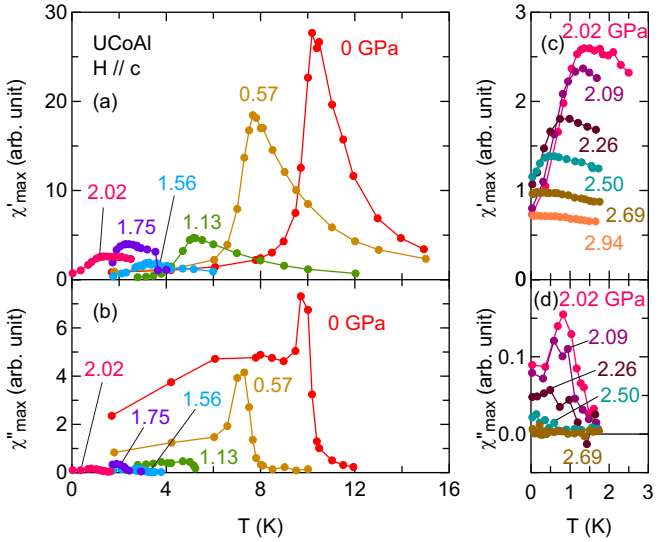

FIG. 4. (Color online) $\chi'_{\rm max}$ and $\chi''_{\rm max}$ as functions of temperature for low pressures (a), (b) and for high pressures (c), (d).

above $T_{\rm cr}$ indicates the crossover. The peak of χ' starts to broaden as the temperature increases beyond $T_{\rm cr}$, as shown in Fig. 3(d), which is characteristic of the crossover nature. This result supports the validity of our estimation for the CP.

B. Pressure dependence of the critical point

Figure 4 depicts $\chi'_{\rm max}$ and $\chi''_{\rm max}$ as functions of temperature under selected pressures. With increasing pressure, the peak position of $\chi'_{\rm max}(T)$ is shifted to lower temperatures. The peak of $\chi'_{\rm max}(T)$ broadens with increasing pressure, as shown in Fig. 4(c). At 2.94 GPa the peak is no longer discernible. The drop of $\chi''_{\rm max}(H)$ is also observed at the peak temperature of $\chi'_{\rm max}(T)$ up to 2.26 GPa and it becomes increasingly obscure with increasing pressure [Fig. 4(d)]. To determine the CP, the peak of $\chi'_{\rm max}$ is more suitable than the drop of $\chi''_{\rm max}(T)$ for high pressures. Accordingly, we define the peak of $\chi'_{\rm max}(T)$ as the CP. We note that the critical divergence of the susceptibility is strongly suppressed with increasing pressure. A distribution of pressure hardly explains this suppression since the drop of $\chi''_{\rm max}(T)$ does not broaden under pressure. Interestingly, such a suppression is also observed in $Sr_3Ru_2O_7$ [18].

In order to determine the QCP, we plot the pressure dependence of $T_{\rm cr}$ in Fig. 5(a). $T_{\rm cr}$ decreases with increasing pressure and its pressure dependence is concave upward. The pressure where $T_{\rm cr}$ goes to zero is estimated to be 2.9 ± 0.2 GPa. The critical field $H_{\rm cr}$ increases and its slope also increases slightly with increasing pressure, as shown in Fig. 5(b). $H_{\rm cr}$ reaches 130 kOe at 2.9 GPa. From these plots, the QCP is determined to be $(P_{\rm QCP}, H_{\rm QCP}) = (2.9 \pm 0.2\ {\rm GPa}, 130 \pm 5\ {\rm kOe})$. The T-P-H phase diagram consequently obtained is shown in Fig. 6.

Our estimation of the QCP greatly differs from $P_{\rm QCP} \approx 1.5$ GPa, as determined by Aoki *et al.* [13]. This discrepancy is attributed to the difference of the definition of the QCP. We consider the pressure where the peak temperature of $\chi'(T)$ goes to zero as the QCP. Here we regard the peak temperature of $\chi'(T)$ as the divergence temperature of the susceptibility. The hysteresis probably vanishes at the same

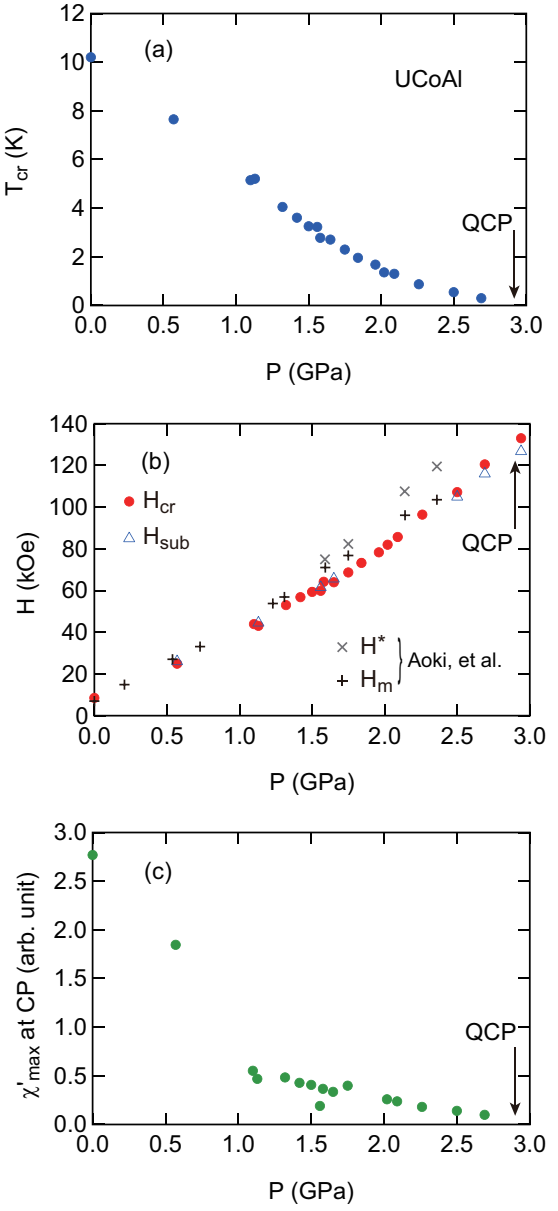

FIG. 5. (Color online) Pressure dependence of characteristic parameters at the CP. (a) Critical temperature $T_{\rm cr}$. (b) Critical field $H_{\rm cr}$ and the subpeak field $H_{\rm sub}$ of $\chi'(H)$ at $T_{\rm cr}$ indicated by closed (red) circles and hollow (blue) triangles. The transition field H_m determined from the magnetostriction and the anomaly field H^* in the transverse MR indicated by plus signs and crosses are cited from Ref. [13]. (c) $\chi'_{\rm max}$.

point. Our determination method is based on a definition of the CP. On the other hand, the previous study estimated the QCP from the pressure dependence of the magnetostriction (see Fig. 6 in Ref. [13]). The amplitude of the jump in the magnetostriction at H_m decreases with increasing pressure and it becomes constant at 1.5 GPa. The transition also starts to broaden from 1.5 GPa. They concluded that these features evidence the QCP to be 1.5 GPa. However, we would like to point out that the data are taken at 2 K, meaning that these features indicate only that $T_{\rm cr}$ is lower than 2 K above 1.5 GPa. This is consistent with our result demonstrated in

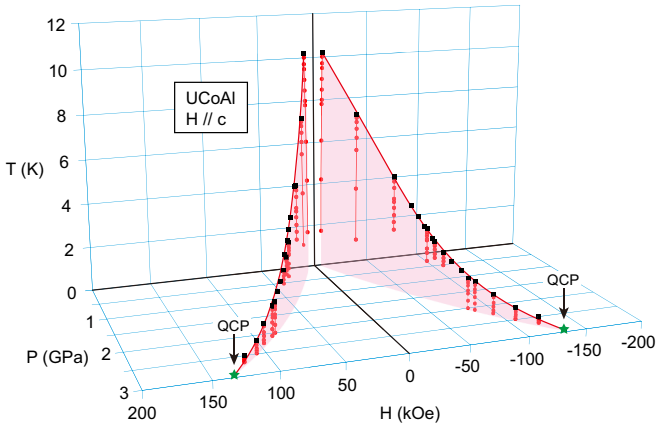

FIG. 6. (Color online) T-P-H phase diagram of UCoAl determined from the ac susceptibility measurements.

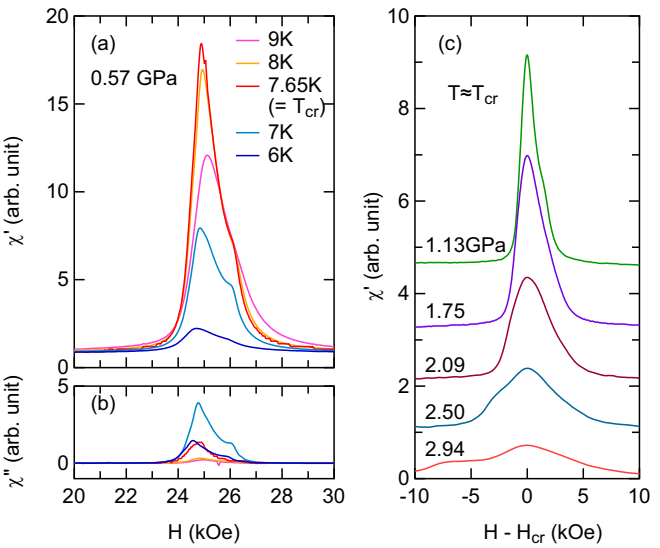

FIG. 7. (Color online) (a) $\chi'(H)$ and (b) $\chi''(H)$ curves for selected temperatures at 0.57 GPa. (c) Pressure evolution of the $\chi'(H)$ curve in the vicinity of H_{cr} at $T \approx T_{cr}$.

Fig. 5(a), which shows that T_{cr} decreases down to 2 K at approximately 1.5 GPa. Note that $H_{cr}(P)$ mostly corresponds to $H_m(P)$ determined from the magnetostriction [13], as shown in Fig. 5(b). This correspondence is quite natural since both the ac susceptibility (above the CP) and magnetostriction are thermodynamic variables. Furthermore, the change in amplitude of the jump does not evidence the criticality of the transition; it merely indicates a change in behavior of the transition. When the pressure increases across the CP, a sharp transition should change to a broad crossover at the CP, after which the jump height of the magnetostriction must continue to smoothly decrease. The change in amplitude of the magnetostriction jump may be associated with the change in $\chi'_{max}(P)$ at the CP, as shown in Fig. 5(c).

The previous study verified the QCP by use of the transverse MR [13]. The peak of the MR at the lowest temperature becomes sharpest at 1.5 GPa and changes to a plateau above this pressure. This may be other evidence that the QCP is located at 1.5 GPa. However, we would like to point out that the MR is not a thermodynamic variable and can be affected by nonthermodynamic factors. In fact, although two kinks of the plateau are observed above 1.5 GPa in the MR, there is no anomaly in the magnetostriction as a thermodynamic variable at the higher field H^* of the kinks [13]. The origin of the peak and plateau in the MR are not fully understood thus far. Therefore, the result from the MR cannot be direct evidence of the QCP. Note that we will demonstrate in the next section that the peak of the longitudinal MR becomes prominent at a slightly higher temperature than the temperature of the CP. The previous study also showed that the A coefficient of the T^2 dependence in the resistivity is enhanced at 1.5 GPa [13]. One may consider this result as evidence of the QCP being located at 1.5 GPa. However, we point out that the A coefficient characterizes a QCP, but its enhancement is not a necessary condition of the QCP.

Finally, we show an anomaly in the ac susceptibility emerging in the vicinity of the CP under pressure. Figures 7(a) and 7(b) show $\chi'(H)$ and $\chi''(H)$ for the selected temperatures at 0.57 GPa. In addition to the main peak, another peak is observed above the main peak field. This subpeak has a similar T dependence to that of the main peak, i.e., the two peaks in χ'' vanish at the same temperature. The subpeak is shifted to the opposite side of the main peak at higher pressures, as shown in Fig. 7(c). The pressure dependence of the subpeak field H_{sub} is also plotted in Fig. 5(b). The appearance of a subpeak may be caused by an inhomogeneity in the pressure. However, this would hardly explain why the position of the subpeak relative to the main peak is switched on an increase in pressure. Note that $H_{sub}(P)$ does not correspond to $H^*(P)$ at which a kink anomaly is observed in the transverse MR [13]. The anomalies at these fields are different in origin. Strikingly, a multipeak behavior is also reported in $Sr_3Ru_2O_7$ [18].

C. Magnetoresistance

First, we show the longitudinal MR as a function of temperature at ambient pressure in Fig. 8(a). At the lowest temperature, $\rho(H)$ shows a steplike increase at about 5 kOe, which is consistent with the previous report and is attributed to the change of the density of states or carrier densities from the paramagnetic to the polarized phase [14]. $\rho(H)$ curves for the up- and down-sweep processes show a hysteresis, as observed in the magnetization process. The hysteresis is gradually diminished with increasing temperature and vanishes at approximately 10 K. Additionally, at this temperature a broad peak of the resistivity develops in addition to the steplike behavior and becomes prominent at approximately 13 K, which is higher than $T_{cr} = 10.2$ K.

The enhancement of the resistivity may evoke additional scattering arising from critical fluctuation of the magnetic moment. We would like to emphasize, however, that the enhancement of the resistivity is not realized in the vicinity of T_{cr} but above T_{cr}, namely, in the so-called "supercritical" region. An unknown scattering mechanism may lie in this region. The evolution of the peak in the resistivity is more apparent at 1.49 GPa, as seen in Fig. 8(b). In the longitudinal MR at 1.5 K the steplike change is accompanied by a small dip at 62 kOe. This behavior is naturally understood by assuming

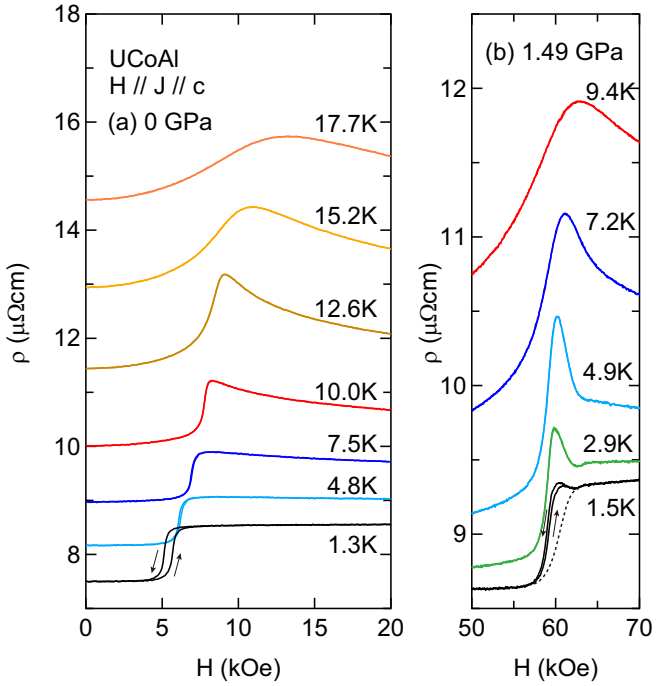

FIG. 8. (Color online) MR $\rho(H)$ for various temperatures at (a) 0 GPa and (b) 1.49 GPa. The magnetic field and electrical current are applied along the c axis. Both increase and decrease processes of the field are plotted. The broken curve in (b) is the expected MR, assuming that additional scattering is absent.

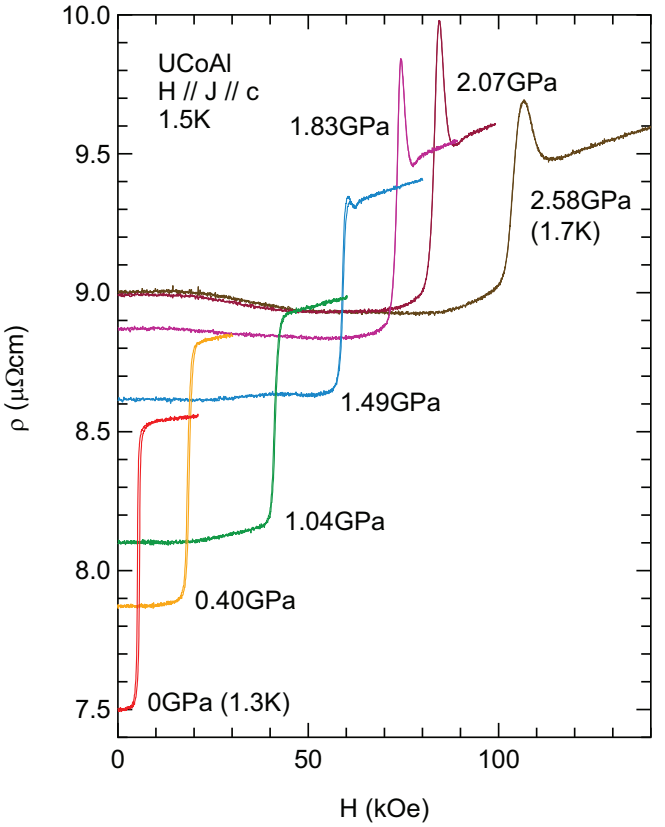

FIG. 9. (Color online) MR $\rho(H)$ for various pressures from 0 to 2.58 GPa. Each curve is plotted at 1.5 K, except for those at 0 GPa (1.3 K) and 2.58 GPa (1.7 K).

an additional peak of the resistivity superimposed upon the steplike MR, indicated by the broken line in Fig. 8(b). The most intense peak is observed at 4.9 K, which is significantly higher than $T_{cr} \approx 2.9$ K. Note that the hysteresis is observed even at 1.5 K, although 1.49 GPa is close to the previous estimation of the QCP located at $P \approx 1.5$ GPa [13].

The behavior of the longitudinal MR $\rho(H)$ varies with increasing pressure. We show the pressure dependence of the $\rho(H)$ curve at approximately 1.5 K in Fig. 9. The hysteresis is observed up to 1.49 GPa as mentioned above but becomes unclear above this pressure. Note that T_{cr} is less than the measurement temperature $T = 1.5$ K above 2.0 GPa, as shown in Fig. 5(a), and that the data above 2.0 GPa are in the crossover (or supercritical) region. (At 1.83 GPa, the hysteresis width becomes too narrow to be observed in the MR.) The steplike increase of $\rho(H)$ is observed up to 1.04 GPa. The peak of the resistivity starts to appear at 1.49 GPa. Its intensity becomes a maximum at 2.07 GPa, and then decreases gradually with further application of pressure. The appearance of the peak above 1.04 GPa is consistent with our suggestion that additional scattering takes place in the supercritical region. The peak does not change to a plateau above 1.5 GPa, as observed in the transverse MR [13]. The anomaly at H^* is not also observed in the longitudinal MR. The appearance of the anomaly may depend on whether the geometrical setup in the MR is longitudinal or transverse. The anomaly associated with the subpeak observed in the ac susceptibility cannot be seen in the longitudinal MR.

Next we show the pressure and field evolutions of $\rho(T)$, especially in the paramagnetic phase. Figures 10(a) and 10(b)

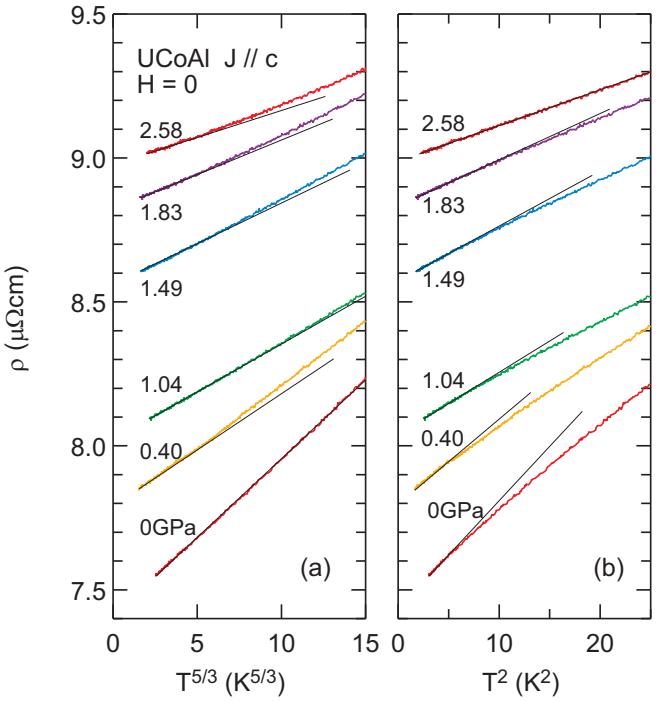

FIG. 10. (Color online) Resistivity as a function of (a) $T^{5/3}$ and (b) T^2 for various pressures at zero magnetic field.

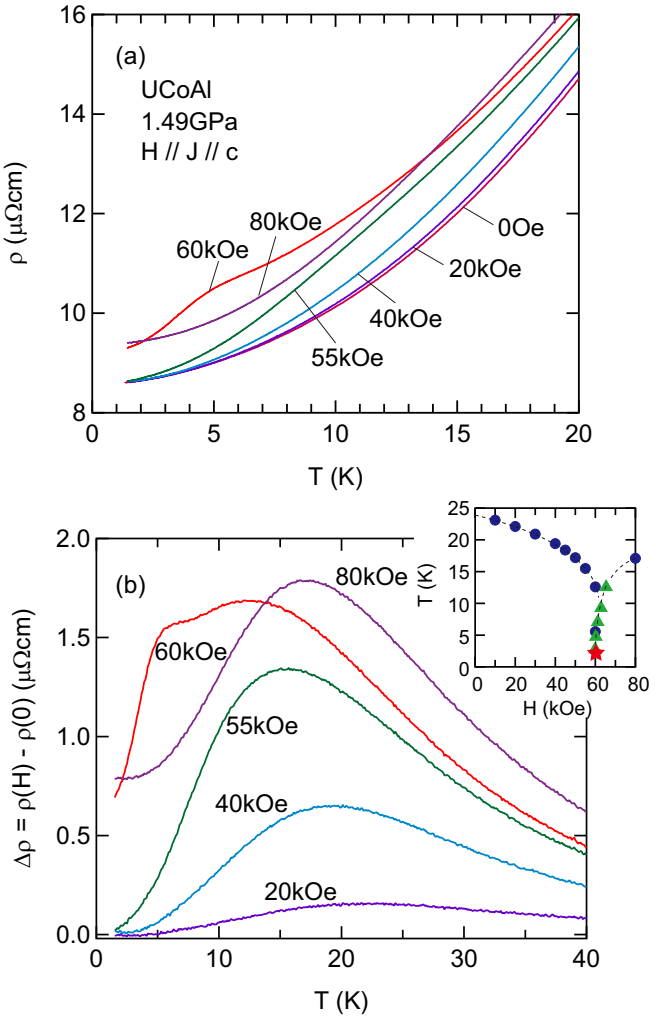

FIG. 11. (Color online) (a) Resistivity $\rho(T)$ under various magnetic fields at 1.49 GPa. (b) Magnetic component of the resistivity $\Delta\rho \equiv \rho(H) - \rho(0)$ as a function of temperature. Inset displays the peak positions in $\Delta\rho(T)$ (closed circles) and in $\rho(H)$ (closed triangles). The CP is indicated by the star.

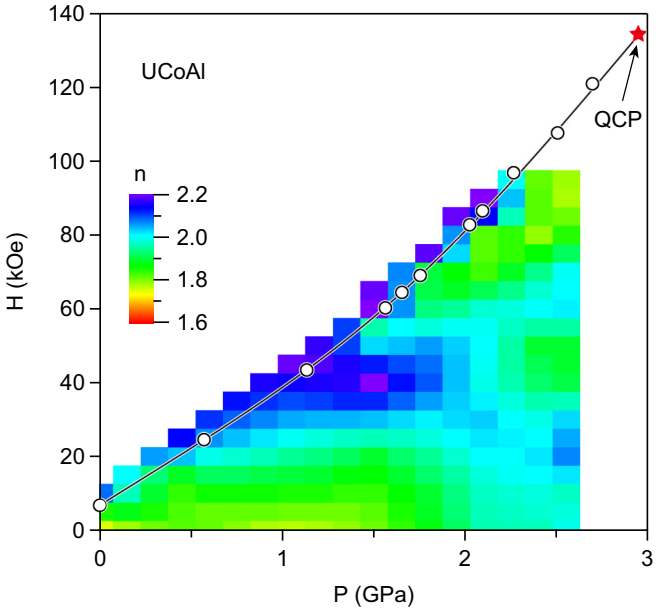

FIG. 12. (Color online) Contour map of the exponent n in the paramagnetic phase. n is derived from a fitting by $\rho(T) = \rho_0 + AT^n$ in the temperature range from 1.5 to 5 K. The plot was constructed by interpolating the results at 0, 0.4, 1.04, 1.49, 1.83, 2.07, 2.42, and 2.58 GPa at magnetic fields from 0 to H_m in ∼10 kOe steps. The hollow circles indicate H_{cr} and the star denotes the QCP.

show the pressure dependence of the resistivity at zero magnetic field as a function of $T^{5/3}$ and T^2, respectively. At 0 GPa, the resistivity obeys a $T^{5/3}$ dependence, indicating the NLMFL behavior [9] arising in the quantum critical regime with ferromagnetic spin fluctuation [19]. This result agrees with the previous report [7]. With increasing pressure, the resistivity deviates from the $T^{5/3}$ behavior and comes to obey T^2 dependence. The FL behavior is recovered as the pressure moves away from the QPTP, which is probably situated at negative pressure [12].

In contrast to its behavior under zero field, $\rho(T)$ under a magnetic field exhibits a complicated evolution. Before showing it, we discuss the behavior of $\rho(T)$ under magnetic fields at 1.49 GPa. As shown in Fig. 11(a), we can see a jump in the resistivity between 55 and 60 kOe at the lowest temperature, which corresponds to the steplike increase of $\rho(H)$ as shown in Fig. 9(b). However, the $\rho(T)$ curve does not change monotonically from 0 to 80 kOe. To emphasize the magnetic field effect, we extract a component of the MR $\Delta\rho \equiv \rho(H) - \rho(0)$ and plot $\Delta\rho$ as a function of temperature in Fig. 11(b). A broad peak near 20 K is revealed. This peak is probably associated with the maximum of the magnetic susceptibility $\chi(T)$ which is commonly observed in itinerant-electron metamagnets. Indeed, in UCoAl, the temperature of the maximum in $\chi(T)$ is $T_0 = 20$ K, and T_0 gradually increases with increasing pressure [12]. The peak temperature decreases with increasing field as does T_0 [20]. Figure 11(b) indicates that the electronic scattering at T_0 is enhanced under magnetic fields.

The peak temperature begins to increase above 60 kOe. As shown in the inset of Fig. 11(b), the peak position of $\Delta\rho$ at 80 kOe seems to connect with the temperature dependence of the peak in $\rho(H)$ shown in Fig. 8(b). Note that the CP at this pressure is located at $(T_{cr}, H_{cr}) = (2.9\ \text{K}, 60\ \text{kOe})$, as indicated by the star in the graph. In Fig. 11(b), the $\Delta\rho(T)$ curve at 60 kOe exhibits another peak at 6 K, which is higher than T_{cr}. This result is consistent with the enhancement of the electronic scattering in the supercritical region discussed above.

The above result tells us that we must pay attention to the $\rho(T)$ data across T_0 or in the supercritical region when we deal with the temperature dependence of the resistivity. For example, the coefficient A of the T^2 term in the resistivity is seemingly enhanced at H_{cr} (= 60 kOe) at 1.49 GPa, since the resistivity at 60 kOe decreases more rapidly with decreasing temperature below 5 K than the others, as seen in Fig. 11(a). However, the apparent enhancement of A is attributed to the additional scattering in the supercritical region. Therefore, this enhancement might not mean mass enhancement of the conduction electron.

Figure 12 displays a contour map of the exponent n estimated from a fitting by $\rho(T) = \rho_0 + A'T^n$ in the

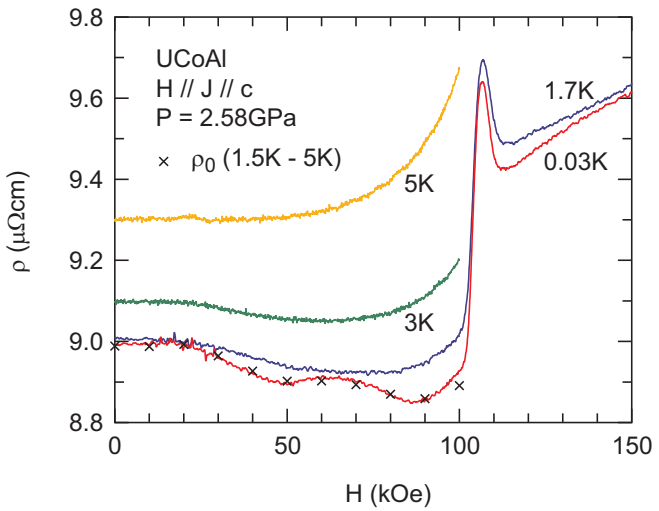

FIG. 13. (Color online) MR for different temperatures at 2.58 GPa. The crosses indicate the residual resistivity ρ_0 estimated from the fitting by $\rho(T) = \rho_0 + AT^n$ in the temperature range from 1.5 to 5 K.

temperature range from 1.5 to 5 K. Here, ρ_0 is the residual resistivity. We do not discuss the data around H_{cr} because the estimated n is affected by the additional scattering as discussed above. The NLMFL behavior is observed in the regions of $0 < P < 2$ GPa and $0 < H < 20$ kOe. Interestingly, other "non-T^2 behavior" regions appear in the paramagnetic state. The first such region is located around the QCP ($P > 2$ GPa and $H > 60$ kOe), where the exponent n is close to 5/3, which implies that the quantum critical regime is arising again in the vicinity of the QCP. The second region is located around $(P, H) \sim (1.5$ GPa,40 kOe), in which n exceeds 2. This pressure corresponds to the *previous* QCP where the enhancement of the A coefficient in the resistivity and change in behavior of the transverse MR are observed [13]. In addition, a great change in the field dependence of the Hall coefficient is also observed at this pressure [21]. The third region is located around $(P, H) \sim (2.5$ GPa,45 kOe), in which n is lower than 2 but still larger than 5/3. This anomaly is probably related to the unusual field dependence of ρ_0 discussed below.

In addition to the complex pressure and field dependences in n, the magnetic field dependence of ρ_0 in the paramagnetic state under pressure is unusual, as seen in Fig. 9. At 0 and 0.4 GPa, $\rho(H)$ for $H < H_m$ is constant. At 1.04 GPa, $\rho(H)$ slightly increases above 20 kOe. Above 1.49 GPa, the $\rho(H)$ curve begins to show a weak decrease above 20 kOe. The magnetic region of this decrease extends to higher fields at higher pressures.

Such complex behavior of the longitudinal MR is more apparent at lower temperatures, especially at pressures near the QCP, as shown in Fig. 13. In contrast to the monotonic behavior in $\rho(H)$ at 5 K, $\rho(H)$ at 0.03 K clearly shows two minima at 48 and 98 kOe. One may expect that rapid decreases of the resistivity at these magnetic fields would be a signature of superconductivity. However, the resistivity does not drop. The MR at 0.03 K agrees with the residual resistivity ρ_0 estimated from the fitting by $\rho(T) = \rho_0 + AT^n$ in the temperature range from 1.5 to 5 K. This indicates that ρ maintains the T^n dependence down to 0.03 K. The "non-T^2" behavior is also observed around these fields, as mentioned above. The unusual field dependence of ρ_0 relates to the complex behavior of n.

IV. SUMMARY

The present study revealed the magnetic T-P-H phase diagram of UCoAl. The QCP is located at $P_{QCP} = 2.9 \pm 0.2$ GPa and $H_{QCP} = 130 \pm 5$ kOe. The previous estimation of $P_{QCP} = 1.5$ GPa does not describe the true QCP, but rather a particular pressure denoted as P^*, where n is unexpectedly enhanced. At this pressure, the enhancement of A in the transverse MR and the drastic change in the field dependence of the Hall coefficient have already been found [13,21]. The other anomaly at H^* also emerges from P^* [13]. To the best of our knowledge, these unique features have apparently not been observed in other itinerant-electron ferromagnets and metamagnets. The origin of these features and the meaning of the point $(T_{cr}(P^*), H_{cr}(P^*))$ are open questions. It is therefore worth emphasizing that the actual phase diagram of itinerant-electron ferromagnets and metamagnets is more complicated than the present model based on Landau theory suggests [22,23]. Considering that characteristic phase diagrams are also revealed in other itinerant-electron magnets, e.g., $Sr_3Ru_2O_7$ [24–26] and $ZrZn_2$ [27,28], the present study corroborates the rich variety of phase diagrams arising in the vicinity of the QPTP and/or QCP.

In addition to the anomalies at P^*, the present study demonstrates some interesting properties: for example, the suppression of the critical divergence in the magnetic susceptibility toward the QCP, the enhancement of the resistivity not at the CP but in the supercritical region, and the unusual temperature dependence of the resistivity in the paramagnetic phase. We expect that the additional critical nature around the CP, especially in the vicinity of the QCP as well as P^*, will be articulated in further studies, and that a different type of magnetic and electronic state in itinerant-electron ferromagnets will thereby be revealed.

ACKNOWLEDGMENTS

We are grateful to N. Tateiwa, K. Ishida, K. Karube, and D. Aoki for helpful discussions. We thank M. Suzuki, M. Kikuchi, H. Moriyama, and N. Fukiage for technical support. This work was supported by Japan Society for the Promotion of Science (JSPS) KAKENHI Grants No. 23654109 and No. 26400345.

[1] N. D. Mathur, F. M. Grosche, S. R. Julian, I. R. Walker, D. M. Freye, R. K. W. Haselwimmer, and G. G. Lonzarich, Nature (London) **394**, 39 (1998).

[2] S. S. Saxena, P. Agarwal, K. Ahilan, F. M. Grosche, R. K. W. Haselwimmer, M. J. Steiner, E. Pugh, I. R. Walker, S. R. Julian, P. Monthoux, G. G. Lonzarich, A. Huxley, I. Sheikin,

D. Braithwaite, and J. Flouquet, Nature (London) **406**, 587 (2000).

[3] N. Huy, A. Gasparini, D. de Nijs, Y. Huang, J. Klaasse, T. Gortenmulder, A. de Visser, A. Hamann, T. Görlach, and H. Löhneysen, Phys. Rev. Lett. **99**, 067006 (2007).

[4] R. A. Borzi, S. A. Grigera, J. Farrell, R. S. Perry, S. J. Lister, S. L. Lee, D. A. Tennant, Y. Maeno, and A. P. Mackenzie, Science **315**, 214 (2007).

[5] S. A. Grigera, R. S. Perry, A. J. Schofield, M. Chiao, S. R. Julian, G. G. Lonzarich, S. I. Ikeda, Y. Maeno, A. J. Millis, and A. P. Mackenzie, Science **294**, 329 (2001).

[6] O. Eriksson, B. Johansson, and M. S. S. Brooks, J. Phys.: Condens. Matter **1**, 4005 (1989).

[7] L. Havela, A. V. Andreev, V. Sechovsky, I. K. Kozlovskaya, K. Prokes, P. Javorsky, M. I. Bartashevich, T. Goto, and K. Kamishima, Physica B (Amsterdam, Neth.) **230**, 98 (1997).

[8] P. Javorský, V. Sechovský, J. Schweizer, F. Bourdarot, E. Lelièvre-Berna, A. V. Andreev, and Y. Shiokawa, Phys. Rev. B **63**, 064423 (2001).

[9] R. P. Smith, M. Sutherland, G. G. Lonzarich, S. S. Saxena, N. Kimura, S. Takashima, M. Nohara, and H. Takagi, Nature (London) **455**, 1220 (2008).

[10] L. Havela, A. Kolomiets, F. Honda, A. V. Andreev, V. Sechovsky, L. E. DeLong, Y. Shiokawa, T. Kagayama, and G. Oomi, Physica B (Amsterdam, Neth.) **281**, 379 (2000).

[11] A. V. Andreev, M. I. Bartashevich, T. Goto, K. Kamishima, L. Havela, and V. Sechovsky, Phys. Rev. B **55**, 5847 (1997).

[12] N. V. Mushnikov, T. Goto, K. Kamishima, H. Yamada, A. V. Andreev, Y. Shiokawa, A. Iwao, and V. Sechovsky, Phys. Rev. B **59**, 6877 (1999).

[13] D. Aoki, T. Combier, V. Taufour, T. D. Matsuda, G. Knebel, H. Kotegawa, and J. Flouquet, J. Phys. Soc. Jpn. **80**, 094711 (2011).

[14] T. D. Matsuda, H. Sugawara, Y. Aoki, H. Sato, A. V. Andreev, Y. Shiokawa, V. Sechovsky, and L. Havela, Phys. Rev. B **62**, 13852 (2000).

[15] M. Endo, N. Kimura, H. Aoki, T. Terashima, S. Uji, T. Matsumoto, and T. Ebihara, Phys. Rev. Lett. **93**, 247003 (2004).

[16] T. D. Matsuda, N. Tateiwa, E. Yamamoto, Y. Haga, Y. Onuki, D. Aoki, J. Flouquet, and Z. Fisk, J. Korean Phys. Soc. **63**, 575 (2013).

[17] K. Karube, T. Hattori, S. Kitagawa, K. Ishida, N. Kimura, and T. Komatsubara, Phys. Rev. B **86**, 024428 (2012).

[18] W. Wu, A. McCollam, S. A. Grigera, R. S. Perry, A. P. Mackenzie, and S. R. Julian, Phys. Rev. B **83**, 045106 (2011).

[19] T. Moriya, *Spin Fluctuations in Itinerant Electron Magnetism* (Springer-Verlag, Berlin, 1985).

[20] T. D. Matsuda, Y. Aoki, H. Sugawara, H. Sato, A. V. Andreev, and V. Sechovsky, J. Phys. Soc. Jpn. **68**, 3922 (1999).

[21] T. Combier, D. Aoki, G. Knebel, and J. Flouquet, J. Phys. Soc. Jpn. **82**, 104705 (2013).

[22] H. Yamada, Phys. Rev. B **47**, 11211 (1993).

[23] D. Belitz, T. R. Kirkpatrick, and J. Rollbühler, Phys. Rev. Lett. **94**, 247205 (2005).

[24] A. M. Berridge, A. G. Green, S. A. Grigera, and B. D. Simons, Phys. Rev. Lett. **102**, 136404 (2009).

[25] A. M. Berridge, S. A. Grigera, B. D. Simons, and A. G. Green, Phys. Rev. B **81**, 054429 (2010).

[26] J. Rech, C. Pépin, and A. V. Chubukov, Phys. Rev. B **74**, 195126 (2006).

[27] N. Kimura, M. Endo, T. Isshiki, S. Minagawa, A. Ochiai, H. Aoki, T. Terashima, S. Uji, T. Matsumoto, and G. G. Lonzarich, Phys. Rev. Lett. **92**, 197002 (2004).

[28] N. Kabeya, H. Maekawa, K. Deguchi, N. Kimura, H. Aoki, and N. K. Sato, J. Phys. Soc. Jpn. **81**, 073706 (2012).